Control of Dispersion of Ni^{2+} Ions via Chelate Ligands in the Preparation of Ni/SiO$_2$ Materials. A XAFS Study

J. Y. Carriat,*,‡ M. Che,*,† M. Kermarec,* M. Verdaguer,§ and A. Michalowicz⊥

*Contribution from the Laboratoire de Réactivité de Surface, URA 1106, CNRS,
Université Pierre et Marie Curie, 75252 Paris Cedex 05, France*

Received July 28, 1997

Abstract: The influence of the Ni deposition mode on the dispersion of Ni^{2+} precursors was investigated in the preparation of Ni/SiO$_2$ catalysts. The coordination sphere of Ni complexes was mainly studied by XAFS spectroscopy in the initial step (dried samples) and after a vacuum activating treatment at 700 °C. Four modes of deposition were compared, two leading to supported silicate phases (exchange with ammine ligands and deposition−precipitation) and the other ones using the ethanediamine ligand (exchange and impregnation modes) which produced isolated Ni^{2+} precursors in electrostatic interaction with the silica support. In this work, EXAFS spectroscopy has been found to be a suitable technique to probe metal−support interactions in the first step of the preparation (dried samples). For samples activated at 700 °C, this spectroscopy showed the presence of several categories of atoms in the first (oxygen backscatterers) and second (Ni and Si backscatterers) shells. A distribution of long ($d \approx 2.04$ Å) and short ($d \approx 1.75$ Å) Ni−O distances was found, corresponding to hexacoordinated (Ni$^{2+}_{6c}$) and isolated tricoordinated (Ni$^{2+}_{3c}$) ions, respectively. Modeling of the structure of the Ni$^{2+}_{3c}$ site indicated a distorted site with two short and one long Ni−O distance. The exchange mode with ethanediamine ligand led to isolated Ni$^{2+}_{3c}$ ions which could then be photoreduced into Ni$^+_{3c}$ ions with the highest yield. Impregnation with ethanediamine Ni nitrate was also found advantageous as it led after thermal activation at 700 °C to NiO particles smaller than those produced from impregnation with Ni nitrate and therefore to smaller Ni particles after the subsequent reduction step.

Introduction

The deposition of transition metal ions onto an oxide support is of fundamental interest to a large variety of chemistry areas such as heterogeneous catalyst preparation,[1] colloid chemistry,[2] geochemistry, and environmental chemistry.[3] This work deals with the deposition of Ni from an aqueous solution of Ni complexes onto a silica support. Several phenomena may occur at this stage: electrostatic adsorption, i.e., formation of an outer-sphere complex; grafting, i.e., formation of an inner-sphere complex with ligands provided by the support; and partial dissolution/reprecipitation of the support in alkaline medium leading to mixed phases[1] (named hereafter phyllosilicates) involving both the metallic cations and ions of the support. The drying step can also be used to control the formation of these

silicate phases by stopping the dissolution of the support. All these features may influence the properties of the final catalyst in the activated or reduced state.[4] The understanding of the mechanism of the deposition of the Ni complex onto the support requires following the modifications occurring in the coordination sphere of the Ni precursor with an appropriate spectroscopy. Therefore, UV−visible Diffuse Reflectance (DRS) and EXAFS spectroscopies have been used. Although the DRS results are only partially referred to in this work since they will be described in a future paper, we show here that *EXAFS is a suitable probe to study metal−support interactions and that the Ni-support bonding step is strongly dependent on the nature of the ligands*.

Previous studies have shown that the conditions of Ni deposition on an oxide support may influence the nature of the supported phase.[5−8] Ni/SiO$_2$ materials prepared by cationic competitive exchange[9,10] and deposition−precipitation[6,11] give rise after drying to supported layered silicates. Such supported

† Institut Universitaire de France.

‡ Present adress: Total, Centre de Recherches, CERT, BP 27, 76700, Harfleur, France.

§ Laboratoire de Chimie des Métaux de Transition, URA 419, CNRS, Université P. et M. Curie, 75252 Paris Cedex 05, France.

⊥ Laboratoire de Physique des Milieux Désordonnés, Faculté des Sciences de l′Université Paris XII, Avenue du Général de Gaulle, 94010, Créteil Cedex, France, and LURE, Université Paris Sud, Bât. 209 D, Campus d'Orsay, 91405 Orsay Cedex, France.

(1) (a) Che, M.; Bonneviot, L. *Pure Appl. Chem.* **1988,** *60,* 1369−1378. Che, M.; Bonneviot, L. *Successful Design of Catalysts*; Elsevier: Amsterdam, 1988; pp 147−158. (b) Che, M. *Studies in Surface Science and Catalysis* Guczi, L. Solymosi, F.; Tetenyi, P., Eds.; Elsevier: Amsterdam, 1993; Vol. 75A, pp 31−67. (c) Dyrek, K.; Che, M. *Chem. Rev.* **1997,** *97,* 305−331.

(2) Davis, J. A.; James, R. O.; Leckie, J. O. *J. Colloid Interface Sci.* **1978,** *63,* 480−499.

(3) Petit, J. C.; Della Mea, G.; Dran, J. C.; Shott, J.; Berner, R. A. *Nature* **1987,** *325,* 705−707. Veblen, D. R.; Banfield, J. F.; Guthrie, G. D., Jr.; Heaney, P. J.; Ilton, E. S.; Livi, K. J. T.; Smelik, E. A. *Science* **1993,** *260,* 1465−1472.

(4) Louis, C.; Cheng, Z. X.; Che, M. *J. Phys. Chem.* **1993,** *97,* 5703−5712. Che, M.; Cheng, Z. X.; Louis, C. *J. Am. Chem. Soc.* **1995,** *117,* 2008−2018.

(5) Tohji, K.; Udagawa, Y.; Tanabe, S.; Ueno, A. *J. Am. Chem. Soc.* **1984,** *106,* 606−612.

(6) Van Dillen, J. A.; Geus, J. W.; Hermans, L. A. M.; Van der Meuden, J. *Proceedings of the 6th International Congress on Catalysis*; Bond, G. C., Wells, P. B., Tompkins, F. C., Eds.; The Chemical Society: London, 1977; p 677.

(7) (a) Hermans, L. A. M.; Geus, J. W. *Preparation of Catalysts II*; Poncelet, G., Grange, P., Jacobs, P. A., Eds.; Elsevier: Amsterdam, 1979; p 131. (b) Burattin, P.; Che, M.; Louis, C. *J. Phys. Chem. B* **1997,** *36,* 7060−7074. (c) Smurov, A. A. *Mem. Soc. Russe Mineral.* **1938,** *67,* 465.

(8) Paulhiac, J. C.; Clause, O. *J. Am. Chem. Soc.* **1993,** *115,* 11602−11603.

(9) Clause, O.; Kermarec, M.; Bonneviot, L.; Villain, F.; Che, M. *J. Am. Chem. Soc.* **1992,** *114,* 4709−4717.

phases decompose upon thermal vacuum treatment at high temperature, leading to the formation of isolated Ni^{2+} ions assumed from DRS data to be tricoordinated (3c) Ni_{3c}^{2+} ions.[12] These ions can be photoreduced by hydrogen into Ni^+ ions,[13,14] which have been found to catalyze the dimerization of olefins.[15] However, with the cationic competive exchange preparation, the amount of Ni^+ ions remains low.[16]

The aim of this work is to control the preparation of Ni/SiO_2 materials by using chelating ligands such as ethanediamine (en) which has been shown to prevent the formation of phyllosilicates and give grafted complexes stable up to 500 °C,[17,18] and to increase after thermally activating treatment the amount of isolated Ni^{2+} precursors and after reduction that of Ni^+ ions.

To this purpose, the modification of the coordination sphere of silica supported Ni^{2+} ions versus the Ni deposition mode was mainly followed by XAFS measurements. Four modes of deposition were selected: competitive cationic exchange in NH_3 and/or in ethanediamine, impregnation with a solution of [Ni (en)_3](NO_3)_2, and deposition−precipitation in urea. The samples were characterized after drying at 80 °C in air and after an activating treatment corresponding to treatment in flowing oxygen at 500 °C and a subsequent treatment in a vacuum at 700 °C. In contrast to what happened in previous studies,[9,11,18] the activated samples remained in vacuum and were never reexposed to air. This procedure was selected to determine the coordination number corresponding to the apparent number of first backscatterers and to check the coordination number 3 assumed from previous work.[12]

The characterization of supported phyllosilicates was investigated by comparison with a reference Ni talc compound hydrothermally synthesized at 500 (crystalline) and 25 °C (ill-crystallized).

Structure of Phyllosilicates

The structure of layered phyllosilicates of talc (2:1 or TOT) and serpentine (1:1 or TO) where T refers to layers of SiO_4 tetrahedra and O to NiO_6 octahedra is well established.[19,20] Ni talc is constituted of a brucite layer with Ni^{2+} ions in octahedral coordination, sandwiched by 2 layers of SiO_4 tetrahedra. The corresponding structural formula is $Si_4Ni_3O_{10}(OH)_2 \cdot nH_2O$. The 1:1 Ni phyllosilicate is built with successive layers of NiO_6 octahedra and SiO_4 tetrahedra.

The structure of Mg talc was investigated by XRD.[21] There exists also a natural Ni talc called willemseite. Mg may be easily substituted by Ni without any structural change.[22] In Ni talc there are 6 oxygen atoms which constitute the first

(10) Kermarec, M.; Carriat, J. Y.; Burattin, P.; Che, M.; Decarreau, A. *J. Phys. Chem.* **1994**, *98*, 12008−12017.

(11) Clause, O.; Bonneviot, L.; Che, M.; Dexpert, H. *J. Catal.* **1991**, *130*, 21−28.

(12) Olivier, D.; Bonneviot, L.; Cai, F. X.; Che, M.; Gihr, P.; Kermarec, M.; Lepetit-Pourcelot, C.; Morin, B. *Bull. Soc. Chim. Fr.* **1985**, 370−380.

(13) Kazansky, V. B.; Elev, I. V.; Shelimov, B. N. *J. Mol. Catal.* **1983**, *21*, 265−274.

(14) Bonneviot, L.; Olivier, D.; Che, M. *J. Mol. Catal.* **1983**, *21*, 415−431.

(15) Lepetit, C.; Kermarec, M.; Olivier, D. *J. Mol. Catal.* **1989**, *51*, 73−93.

(16) Bonneviot, L.; Cai, F. X.; Che, M.; Kermarec, M.; Legendre, O.; Lepetit, C.; Olivier, D. *J. Phys. Chem.* **1987**, *91*, 5912−5921.

(17) Bonneviot, L.; Clause, O.; Che, M.; Manceau, A.; Dexpert, H. *Catal. Today* **1989**, *6*, 39−46.

(18) Clause, O.; Bonneviot, L.; Che, M. *J. Catal.* **1992**, *138*, 195−205.

(19) Bailey, S. W. *Crystal Structures of Clay Minerals and their X-Ray Identification*; Brindley, G. W., Brown, G., Eds.; Mineralogical Society: London, 1980; pp 6−46.

(20) Ruclidge, J. C.; Zussman, J. *Acta Crystallogr.* **1965**, *19*, 381−389.

(21) Rayner, J. H.; Brown, G. *Clays Clay Miner.* **1973**, *21*, 103−114.

(22) Macksimovic, Z. *Zap. Miner. Obsh.* **1973**, *102*, 143−149.

backscatterers at about 2.05 Å of Ni and 6 Ni and 4 Si atoms as next nearest backscatterers at about 3.10 and 3.25 Å of Ni, respectively.

In the group of serpentine, the lizardite corresponds to an orthoserpentine with plane layers. When the substitution of Mg by Ni is larger than 50%, these minerals are called nepouite.

Experimental Section

Sample Preparation. The silica support was generally a Spherosil XOA 400 supplied by Rhône Poulenc France ($S_{BET} = 356$ m²·g⁻¹, pore volume = 1.25 cm³·g⁻¹, average pore diameter = 80 Å). For samples prepared by exchange in en, a nonporous silica was employed: Aerosil A 380 (supplied by Degussa, Germany, purity >99.5%, $S_{BET} = 380$ m²·g⁻¹).

We have limited the Ni loading of the samples to 1.4 to 2.1% since previous studies showed that the reduction degree in Ni^+ ions strongly decreased when the Ni loading increased.[12]

(*a*) *Competitive Cationic Exchange in Ammonia Aqueous Solutions*: *ENi(NH₃)*. A 2.5 g sample of silica was put in contact with 50 mL of a solution containing 0.1 M $Ni(NO_3)_2 \cdot 6H_2O$ and 0.8 M NH_4-NO_3 in a controlled temperature vessel at 25 °C. The suspension was magnetically stirred for 24 h and the pH was adjusted to 9.8 by bubbling gaseous ammonia. The solid was then filtered, washed three times with 50 mL of distilled water, and dried in an oven at 80 °C for 24 h. For the sake of brevity, this sample is referred to as ENi(NH₃)-80 where E stands for exchange. The Ni loading is 1.4 wt %.

(*b*) *Deposition Precipitation in Urea Aqueous Solutions*: *DPU*. This procedure was described by Hermans and Geus.[7a] A 7.6 g sample of silica was put in contact with a 500 mL solution containing 0.14 M $Ni(NO_3)_2 \cdot 6H_2O$, 0.42 M $(NH_2)_2CO$ (urea), and 0.02 M HNO_3. The suspension was kept in a controlled temperature vessel at 90 °C for 1 h. The mixture was then cooled to 25 °C to solubilize nickel carbonates and basic nitrates formed during the preparation.[7b,c] The sample was filtered, washed three times with 100 mL of distilled water, and then dried in an oven at 80 °C for 24 h. This sample is referred to as DPU-80 where U stands for urea. The Ni loading is 2.1 wt %.

(*c*) *Incipient Wetness Impregnation in Ethanediamine Aqueous Solutions*: *INi(en)*. A 5 g sample of silica was impregnated with a solution containing 0.24 M $Ni(NO_3)_2 \cdot 6H_2O$ and 0.72 M $NH_2(CH_2)_2$-NH_2. The volume used corresponds to 1.18 mL·g⁻¹ of silica. The impregnated silica was kept in a desiccator for 2 h to ensure an homogeneous distribution of the solution within the pores of the support. The sample was then dried in an oven at 80 °C. This sample is referred to as INi(en)-80 where I stands for impregnation. The Ni loading is 1.5 wt %.

(*d*) *Exchange in ethanediamine aqueous solutions*: *ENi(en)*. A 5 g sample of silica was added to 100 mL of a solution containing 0.3 M $Ni(NO_3)_2 \cdot 6H_2O$, 1.3 M NH_4NO_3, and 0.9 M $NH_2(CH_2)_2NH_2$. The pH of the solution was kept at 10 by bubbling gaseous ammonia. The suspension was stirred for 2 h. The sample was filtered, washed three times with 100 mL of water, and then dried at 80 °C according to the same procedure as above. This sample is referred to as ENi(en)-80. The Ni loading is 1.5 wt %.

Sample Pretreatment. Samples dried at 80 °C in air were first submitted to flowing oxygen treatment at 500 °C for 2 h, to remove the ammine and the ethanediamine ligands or to decompose the urea for the ENi(NH₃), ENi(en), and DPU samples, respectively. The absence of reduction of the Ni^{2+} ions after such a treatment was checked by EPR and ferromagnetic resonance measurements. For ENi(en), the first and second (respectively N and C) backscatterers are eliminated and Ni^{2+} ions bind to the oxygen atoms of the support. DRS and EXAFS analysis were performed after this oxygen pretreatment but the corresponding results are not reported in this paper. Then, a vacuum treatment up to 700 °C for 15 h was performed. This last procedure will be referred to as the activating treatment. In the subsequent sections (vide infra), the different samples will be analyzed after drying in air at 80 °C (*dried samples*) and after the activating treatment (*activated samples*).

Special cells allowed the transfer of the samples activated in the laboratory to the EXAFS chamber, without any reexposure to air.

XAFS Measurements. EXAFS measurements at the Ni K edge were performed at the LURE synchrotron radiation facility (Orsay, France) with use of the D13 X-ray Absorption port of the DCI storage ring (positron energy 1.85 eV; mean ring current 300 mA). The spectra were recorded at room temperature in the transmission mode by using two air-filled ionization chambers. A double crystal Si(311) monochromator was used. For EXAFS measurements, the energies were scanned with 2 eV steps from 8200 to 9200 eV, while for XANES they were scanned with 0.2 eV (and 0.1 eV for the preedge range) steps in the 8300–8450 eV range. The energy was calibrated by using a Ni metal foil reference. The Ni talc and nepouite reference samples were ground and homogeneously dispersed in cellulose pellets while the dried and activated supported samples were inserted between two Kapton windows in special cells allowing sample transfer and recording of the spectra under vacuum.[23] In this case, the sample thickness could not be perfectly controlled and thus systematic errors in the EXAFS amplitudes could not be completely avoided. EXAFS measurements were performed three times on each sample. Data analysis was performed with the use of the "EXAFS pour le Mac" package.[24] The $\chi(k)$ functions were extracted from the data by using a linear preedge background and a combination of polynomials and spline atomic absorption background. $k = [8\pi^2 m_e(E - E_o)/h^2)]^{1/2}$ where E_o is the energy threshold, taken at the inflection point of the absorption edges. E_o has been corrected for each spectrum in the fitting procedure.

The Fourier transforms (FT) were calculated on $w(k)k^3\chi(k)$ where $w(k)$ is a Kaiser–Bessel window with a smoothness parameter equal to 2.5. The k limits are equal to 2–13 Å^{-1}. In this work, all FT are calculated and presented without phase correction.

It was checked on the spectrum of crystalline talc that multiple scattering contributions in the 0–3.5 Å distance range were negligible. Single scattering fits of experimental curves to theoretical models were performed on filtered spectra in two steps: (i) fitting of the Ni–O shell alone (filtering domain: 0.7–2.1 Å) and (ii) fitting of the total spectrum within 0–3.5 Å (Ni–O, Ni–Ni + Ni–Si shells). The number of independent points in the filtered spectra is $N_{ind} = 2\ \Delta R \Delta k/\pi$.

We have used the standard EXAFS formula:

$$k\chi(k) = -S_o^2 \sum_i \frac{N_i}{R_i^2} |f_i(k,R_i)| e^{-2\sigma i^2 k^2} e^{-2R_i/\lambda_i(k)} \sin(2kR_i + \phi_i(k,R_i))$$

where the summation is performed over all the filtered contributions. S_o^2 is the inelastic reduction factor ($S_o^2 = 1$ in our fits), N_i is the number of backscatterers at a distance R_i from the central Ni atom, σ_i is the Gaussian Debye–Waller factor for the backscatterers i, and $\lambda_i = (k/\Gamma_i)$ is the mean free path of the photoelectron.

Ab initio amplitude and phase functions $|f_i(k,R_i)|$ and $|\phi_i(k,R_i)|$ were calculated by using FEFF6 program of the university of Washington.[25] Following the Report of the International Workshop on Standards and Criteria in XAS,[26] the error bars on fitted parameters were estimated by using standard statistical procedures.[27] The signal-to-noise ratio used to estimate the experimental noise in the data was determined by two methods: (i) a statistical treatment of the several available data and (ii) a Fourier analysis of the noise. It was checked that both methods give similar results. The "goodness" of the fits is evaluated by two numbers: (i) The agreement factor ρ (%) = $\sum[k\chi_{th}(k) - k\chi_{exp}(k)]^2/\sum[k\chi_{exp}(k)]^2$ and (ii) the fit quality factor $\chi_\nu^2 = \sum[k\chi_{th}(k) - k\chi_{exp}(k)]^2/(e^2 \cdot \nu)$, where e is the average experimental signal error bar and ν is the degree of freedom of the fit. When two fitting models are compared, the final choice is guided by the F test analysis[27] where

$$F = \chi_\nu(\text{Fit 1})/\chi_\nu(\text{Fit 2})$$

Since they are highly correlated, N_i, σ_i, and Γ_i amplitude parameters of each shell could not be fitted all together. It was necessary to determine the values of Γ_i on a model compound, where the numbers of neighbors are known, and to use these values as fixed parameters in the fitting of the other spectra. A similar procedure was used to determine the value of ΔE_o, the threshold energy correction, to fit the distances for the unknown compounds. In this study we have used the crystalline Ni talc synthesized at 500 °C, referred to hereafter as Ta-500, as the model compound. With the use of FEFF phases and amplitudes, we have found that a good fit could be reached if the Γ_i values of the three Ni–O, Ni–Ni, and Ni–Si shells are different and kept equal to the values found for the Ta-500 model compound in fitting the unkown compounds (Tables 1 and 2). The ΔE_o correction for each shell is determined on the model compound in order to obtain R values closest to the crystal structure (R_{Ni-O} = 2.07 Å, R_{Ni-Ni} = 3.05 Å, R_{Ni-Si} = 3.25 Å). For the unknown compounds under study, only $\Delta E_{o(Ni-O)}$ is fitted. Then the energy shifts $[\Delta E_{o(Ni-Ni)} - \Delta E_{o(Ni-O)}]$ and $[\Delta E_{o(Ni-Si)} - \Delta E_{o(Ni-O)}]$ are constrained to be constant and equal to the values found for Ta-500. This method permits the number of free parameters to be decreased and the statistics of the fit to be improved.

Despite these constraints, we have found that the amplitude parameters for Ni–Ni and Ni–Si shells remained strongly correlated. The validity of the number of Si determined by the fitting will be discussed in the next section.

Results

(A) EXAFS Analysis. (1) Reference Compounds: Ta-500 and Ta-25. It is known that the structure of a crystalline talc is not modified when Mg is substituted by Ni. Using the crystal structure given by Rayner and Brown[21] for the Mg talc structure, we have calculated the FEFF EXAFS spectra of Ni talc with single scattering paths only or including multiple scattering contributions. Figure 1 reports the imaginary part Im[$F(R)$] of these theoretical Fourier transform spectra. It appears that up to 3.5 Å, which corresponds to a distance larger than that of the Ni and Si second and third neighbors, the multiple scattering may be neglected. Hence, the calculations for all samples have been carried out by using the single scattering model.

The EXAFS and Fourier transforms of the reference compounds are shown in Figure 2, parts A and B, respectively. The fitted structural parameters are reported in Table 1.

Except for their relative amplitudes, Ta-25 and Ta-500 spectra present the same features with the same frequencies, thus indicating the same structure for the ill-crystallized compound as that of Ta-500, as already known from the litterature.[28] The Fourier transforms exhibit two main peaks at around 1.7 and 2.8 Å, corresponding to the nearest O backscatterers and to the Ni and Si next nearest backscatterers, respectively. A third contribution at around 5.7 Å is also observed. As expected for an ill-crystallized compound, owing to an increased disorder, the amplitudes are lower for Ta-25 and mainly for the second peak. Table 1 shows an increased value of the Debye–Waller factor σ for the O and Ni contributors. The decrease of the number of Si backscatterers is stronger than that observed for Ni. However, the error bar for σ_{Si} is important, thus indicating the difficulty in determining with accuracy the number of Si backscatterers. This trend will be confirmed for all other compounds (Tables 1 and 2).

The decrease in the number of backscatterers could be also interpreted by a smaller size of particles, which involves a decrease of the coordination number for the second neighbors.[29–32] This could be due to the higher proportion of surface atoms in

(23) Carriat, J. Y. Thesis, 1994, Université P. et M. Curie.

(24) Michalowicz, A. EXAFS pour le Mac, Logiciels pour la Chimie. *Soc. Fr. Chim., Paris* **1991**, 102–103.

(25) Rehr, J. J.; Mustre de Leon, J.; Zabinski, S. I.; Albers, R. C. *J. Am. Chem. Soc.* **1991**, *113*, 5135–5140. Mustre de Leon, J.; Rehr, J. J.; Zabinski, S. I.; Albers, R. C. *Phys. Rev. B* **1991**, *44*, 4146–4156.

(26) Lytle, F. W.; Sayers, D. E.; Stern, E. A. Report of the International Workshop on Standards and Criteria in X-Ray Absortion Spectroscopy, *Physica* **1989**, B*158*, 701.

(27) Bevington, P. R. *Data Reduction and Error Analysis for the Physical Sciences*; McGraw-Hill: New York, 1992; pp 205–209.

(28) Montdesir, H. Thesis 1987, Université Paris-Sud.

(29) Greegor, R. B.; Lytle, F. W. *J. Catal.* **1980**, *63*, 476–486.

Table 1. Fitted Structural Parameters for Reference Compounds and Dried Ni/SiO$_2$ Materials as Determined by EXAFS at the Ni K Edge[a,b]

sample	backscatterer	N	$10^2\,\sigma$	Γ	R (Å)	ΔE^0 (eV)	ρ^* (%)
Ta−500	O	6(0)	5.8(0.8)	0.90(0.05)	2.05(0.01)	−0.7(0.6)	
	Ni	6(0)	7.1(0.8)	0.72(0.3)	3.05(0.02)	−2.7(2.1)	0.22
	Si	4(0)	7.1(4)	0.38(0.1)	3.24(0.06)	−4.6(2.2)	
Ta−25	O	7.0(2)	8.6(0.8)	0.90(0)	2.05(0.01)	−0.7(0.5)	
	Ni	5.3(1.6)	8.8(1.7)	0.72(0)	3.09(0.02)	−1.3(0)	0.13
	Si	2.4(0.8)	6.9(9.3)	0.38(0)	3.21(0.02)	−3.2(0)	
Ne−150	O	7.2(0.5)	8.8(0.5)	0.90(0)	2.04(0.00)	0.2(0.3)	
	Ni	7.0(0.8)	9.7(0.7)	0.72(0)	3.09(0.01)	−1.8(0)	0.28
	Si	2.4(0.2)	1.7(3.5)	0.38(0)	3.23(0.01)	−3.6(0)	
DPU−80	O	7.2(1.7)	8.4(0.5)	0.90(0)	2.04(0.00)	−1.1(0.3)	
	Ni	5.0(1.3)	7.6(1.2)	0.72(0)	3.09(0.01)	−3.1(0)	0.03
	Si	3.9(1.4)	10.3(4.1)	0.38(0)	3.25(0.02)	−4.9(0)	
ENi(NH$_3$)−80	O	7.4(1.5)	8.6(0.5)	0.90(0)	2.05(0.00)	−1.1(0.3)	
	Ni	5.1(0.8)	8.7(0.5)	0.72(0)	3.09(0.01)	−3.1(0)	0.23
	Si	3.0(0.5)	7.9(3.6)	0.38(0)	3.23(0.02)	−5.0(0)	
ENi(en)−80	N	5.6(0.4)	9.5(0.85)	0.52(0)	2.09(0.01)	5.0(0.4)	0.37
INi(en)−80	N	6.3(0.7)	9.9(1.6)	0.52(0)	2.11(0.02)	4.2(0.9)	0.55
Ni(en)$_3$(NO$_3$)$_2$	N	6.00	9.6	0.52	2.12	3.7	0.30

[a] N, σ, Γ, R, ΔE°, and ρ^* stand for the coordination number, the Debye−Waller factor, the mean free path factor, the radial distance, the energy threshold correction in comparison to the energy threshold E°, and the agreement factor, respectively. E° values were taken in the 8336−8342 eV range. The signal-to-noise ratio varied from 8.6 (Ta-25) to 25.5 (Ta-500). [b] The error is given in parentheses. The (0) corresponds to fixed parameters as discussed in the experimental part.

Table 2. Fitted Structural Parameters for Ni/SiO$_2$ Materials Activated at 700 °C, as Determined by EXAFS at the Ni K Edge[a−d]

sample	backscatterer	N	$10^2\,\sigma$	Γ	R (Å)	ΔE^0 (eV)	ρ^* (%)
DPU−700	O$_{(1)}$	2.7(0.2)	9.1(1)	0.9(0)	2.02(0.01)	−1.0(0.7)	
	O$_{(2)}$	0.5(0.1)	4.9(4)	0.9(0)	1.75(0.02)	−1.0(0.7)	
	Ni	3.2(2.2)	12(1.0)	0.7(0)	2.97(0.02)	−3.0(0)	0.43
	Si	1.6(0.5)	10.9(9.4)	0.4(0)	3.12(0.17)	−5.0(0)	
ENi(NH$_3$)−700	O$_{(1)}$	2.3(0.2)	9.0(1)	0.9(0)	2.04(0.01)	0.9(0.8)	
	O$_{(2)}$	0.4(0.1)	3.9(6)	0.9(0)	1.76(0.03)	0.9(0.8)	0.39
	Ni	2.9(1.7)	13.6(2.8)	0.7(0)	2.97(0.02)	−1.1(0)	
	Si	1.1(0.4)	8.0(4.0)	0.4(0)	3.18(0.13)	−3.1(0)	
INi(en)−700	O$_{(1)}$	2.9(0.5)	11.1(1.7)	0.9(0)	2.00(0.09)	−0.2(1.1)	
	O$_{(2)}$	0.4(0.2)	2.4(11.0)	0.9(0)	1.74(0.03)	−0.2(0)	0.22
	Ni	2.7(1.0)	8.9(1.6)	0.7(0)	2.94(0.01)	−2.2(0)	
	Si	1.7(0.8)	12.5(11.6)	0.4(0)	3.10(0.03)	−4.1(0)	
ENi(en)−700[d]	O$_{(1)}$	1.0(0.8)	8.3(9.6)	0.9(0)	1.95(0.12)	−0.8(3.1)	
	O$_{(2)}$	1.2(0.3)	5.2(3.4)	0.9(0)	1.75(0.01)	−0.8(0)	0.33
	Ni	5.2(4.9)	18.3(2.2)	0.7(0)	2.91(0.03)	2.5(0)	7.05
	Si	0.7(0.2)	7.1(3.7)	0.4(0)	3.10(0.03)	−2.5(0)	7.14

[a] N, σ, Γ, R, ΔE°, and ρ^* stand for the coordination number, the Debye−Waller factor, the mean free path factor, the radial distance, the energy threshold corrections in comparison to the energy threshold E°, and the agreement factor, respectively. E° values were taken in the 8334−8339 eV range. The signal-to-noise ratio varied from 6,7 (DPU-700) to 8.9 (ENi(en)-700. [b] The error is given in parentheses. The (0) correspond to fixed parameters as discussed in the experimental part. [c] For the first three samples, the Ni−O shell was first fitted and the values found for O$_{(1)}$ and O$_{(2)}$ were introduced as fixed parameters for the fitting of the (Ni−O + Ni−Ni + Ni−Si) shells. [d] For the ENi(en)-700 sample, as the EXAFS signal for the Ni−Ni + Ni−Si contributions was very weak, the Ni or Si contribution was fitted alone in the second shell.

comparison with core atoms. We can now discuss these effects in terms of disorder and/or reduced coordination numbers.

It is well-known that EXAFS analysis of pure metallic first shells in metallic clusters may provide quite accurate values of the variation of the coordination numbers and Debye−Waller factors. Unfortunately, the disorder effects measured by EXAFS on the second shell of atoms surrounding Ni ions are certainly less accurate as this shell involves a mixing of two types of atoms. In addition, the theoretical Si EXAFS signal is very weak as compared to that of Ni. In our fits, we let the coordination numbers N and Debye−Waller factors σ free since the total number of fitted parameters was still less than the degree of freedom. However, we think that the values obtained for N and σ are not totally relevant because in such a complicated fit, these numbers are strongly correlated. They

just reflect that the total amplitude of the second peak decreases, suggesting some qualitative local disorder. This local disorder can be due either to size effects or to structural distortions. Both possibilities are compatible with the analysis of our data.

(2) Silica-Supported Ni Materials. (2.1) Dried Materials. (a) Supported Phyllosilicates: DPU-80 and ENi(NH$_3$)-80. During the deposition step, the Ni complexes are hydrolyzed and give rise to supported phyllosilicates after olation reactions[1b,10] with the OH groups of silica. A recent IR study has shown that DPU-80 and ENi(NH$_3$)-80 correspond to phyllosilicates of nepouite and talc-like structure, respectively.[10] These structures do not have residual NH$_3$ molecules. This is the reason why the first shell was fitted with O atoms only.

The EXAFS spectra for these samples (Figure 3A) have been compared to the corresponding model compounds Ne-150 and Ta-25. The choice of a nepouite synthesized at 150 rather than at 25 °C is justified by the fact that deposition−precipitation is performed at 90 °C, leading to a slightly better crystallized sample. The EXAFS spectra for the supported and model

(30) Kip, B. V.; Duivenvoorden, F. B.; Koeningsberger, D. C.; Prins, R. *J. Catal.* **1987**, *105*, 26−38.

(31) Mizushima, T.; Tohji, K.; Udagawa, Y.; Harada, M.; Ishikawa, M.; Ueno, A. *J. Catal.* **1988**, *112*, 282−289.

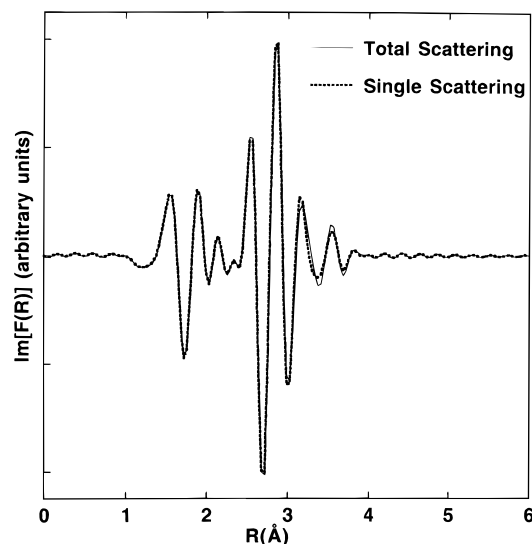(32) Manceau, A.; Calas, G. *Clay Miner.* **1986**, *21*, 341−360.

XAFS Study of Dispersion of Ni^{2+} Ions on Silica

J. Am. Chem. Soc., Vol. 120, No. 9, 1998 2063

Figure 1. Imaginary part of the calculated Fourier transforms of Ni talc, using single and multiple scattering paths.
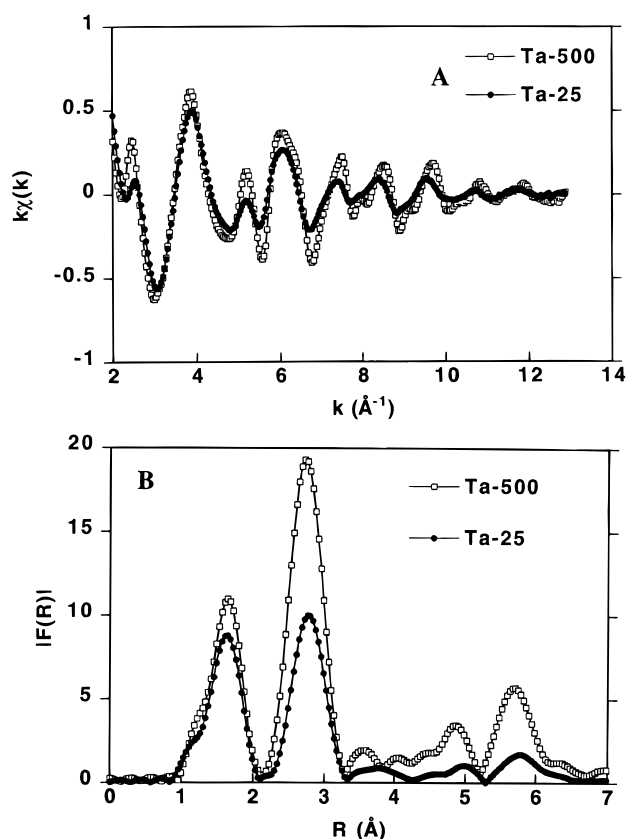

Figure 2. EXAFS signals (A) and Fourier transforms (B) of Ta-500 and Ta-25 samples.

compounds cannot be discriminated. It appears that spectral fluctuations due to experimental errors are more important than the difference observed in the spectra series of these compounds: although the number of Si backscatterers are different, EXAFS spectra of DPU-80, ENi(NH$_3$)-80, Ta-25, and Ne-150 are almost identical, their differences being within the error bars. Figure 3B shows the similarity of the Fourier transforms for these samples. At first view, the amplitude of the second peak suggests the similarity of DPU-80 and ENi(NH$_3$) with Ne-150 and Ta-25, respectively.

Table 1 shows that for these supported phyllosilicates, the distances for the O, Ni, and Si backscatterers are in agreement
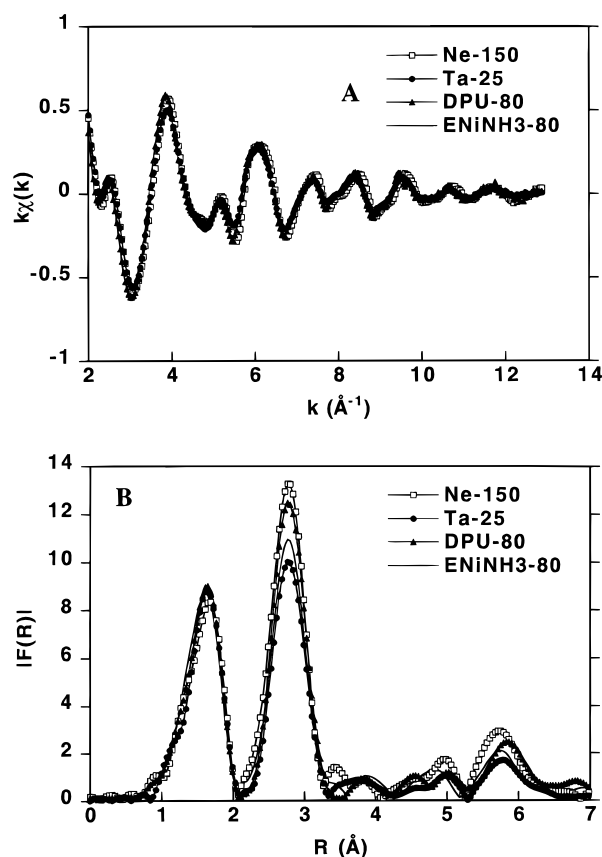

Figure 3. EXAFS signals (A) and Fourier transforms (B) of model compounds Ta-25 and Ne-150 and supported phyllosilicates DPU-80 and ENi(NH$_3$)-80.

with the expected distances observed for phyllosilicates of talc or serpentine structure.[21,32] The number of O backscatterers is shown to increase as well with the σ factor to a value larger than the theoretical one. These uncertainties due to the correlations between N and σ are worsened by the increase of the experimental noise. For both supported samples, the apparent number of Ni backscatterers decreases in comparison with that observed for Ta-500 and is consistent with an ill-crystallized structure. However, it may be noticed that the number of Si backscatterers for DPU-80 whose structure corresponds to an ill-crystallized nepouite[10,33] is superior to the value expected for a crystalline nepouite (2 Si at 3.25 Å).

In the preceding section, we have already underlined the difficulty in obtaining pertinent numbers of Si backscatterers by fitting the EXAFS spectra of compounds of phyllosilicate-like structure. Since the theoretical Si EXAFS signal is very weak as compared to that of Ni, variations of N$_{Si}$ in the 2−4 range give rise to very small variations of the simulated spectra, within the error bars. For this reason, the discrimination by EXAFS spectroscopy between ill-crystallized compounds of talc and nepouite-like structure does not appear to be relevant in the experimental conditions we used. However, although the quantitative estimation of Si neighbors in phyllosilicates is difficult, EXAFS is a good qualitative probe to detect the presence of Ni and Si backscatterers.

(b) INi(en)-80 and ENi(en)-80. The spectra (EXAFS and Fourier transforms) of samples prepared by impregnation or by exchange using ethanediamine ligand are shown to be almost identical to that of Ni(en)$_3$(NO$_3$)$_2$ salt (Figure 4, spectra A and B). The EXAFS signals appear dominated by a single mona-
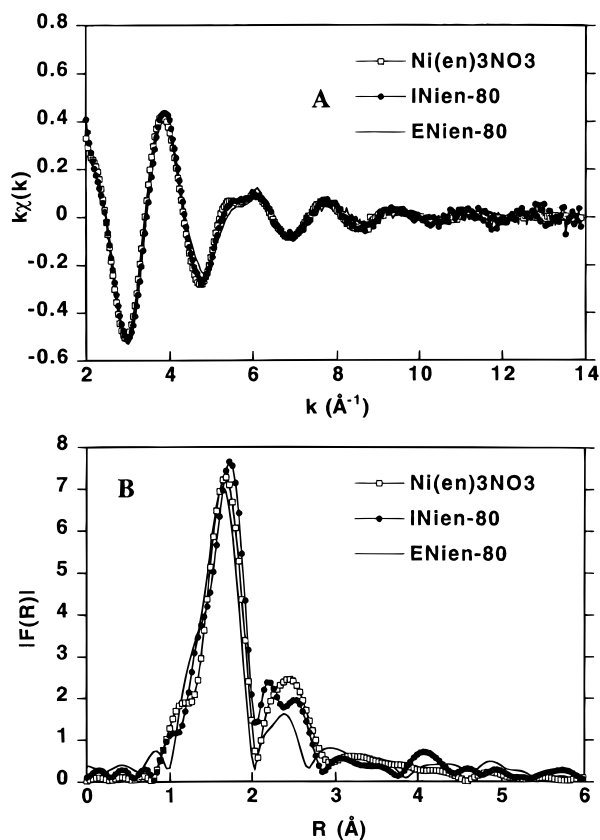
(33) Burattin, P. Thesis, 1994, Université P. et M. Curie.

Figure 4. EXAFS signals (A) and Fourier transforms (B) of [Ni(en)$_3$]-(NO$_3$)$_2$, INi(en)-80, and ENi(en)-80.

tomic first shell (N backscatterers) with a weak second shell contribution (C backscatterers). This result shows that Ni $^{2+}$ ions are still complexed with ethanediamine and may thus be considered as isolated one from another. A slight but nonsignificant modification of the site appears for supported samples when considering the weak signal of the second shell. The Ni−N distances (2.09 and 2.11 Å) are in agreement with those found for the crystal structure of the ethanediamine nitrate[34] (Table 1). In contrast to ammine ligands, the use of ethanediamine leads to Ni complexes in electrostatic interaction with the support and inhibits the formation of supported phyllosilicates.

(2.2) Influence of the Activation Treatment at 700 °C. The results (EXAFS signals and Fourier transforms) comparing the four samples before preteatment (*dried samples*) and after a vacuum activating pretreatment (*activated samples*) are gathered in Figure 5. Figure 6 shows samples after activating treatment at 700 °C. For the sake of clarity, DPU-700 data were not included in this figure as this sample gives a similar spectrum as ENi(NH)$_3$-700. Table 2 reports on the values of the fitted structural parameters.

(a) DPU-700 and ENi(NH$_3$)-700. The EXAFS results are similar for both compounds. The EXAFS spectra (Figure 5A, full circles) show smaller oscillations similar to those observed for dried materials for *k* values <8 Å^{-1} (empty squares). The Fourier transforms of these pretreated samples (Figure 5B) show two main peaks around 1.7 and 2.8 Å corresponding to those already observed for the dried materials, but with much lower amplitudes.

The peak at 5.8 Å is no longer observed. The disappearance of this peak and the strong decrease of the overall amplitude

indicate that these compounds are disordered. In the 1−2 Å region corresponding to the first shell, one may observe a smaller peak around 1.2 Å (Figure 6B). In agreement with the EXAFS spectra, *the first shell could only be correctly fitted by assuming the existence of two types of oxygen atoms*, O$_{(1)}$ at 2.04 and O$_{(2)}$ at 1.76 Å, respectively (Table 2). More precisely, it was possible to compare the fit of the Ni−O shell including either two oxygen atoms or only one. The F test indicated with an 85% probability level that the two oxygen shell fit is better than that with the one oxygen shell. The results are almost equivalent for both samples, the number of O$_{(1)}$ atoms being predominant.

The second shell was also modeled with Ni and/or Si contributors. The F test for these fits showed with a probability of 80% that a mixture of both contributors is necessary. In the second shell, a strong decrease of the apparent number of Ni and Si atoms was also observed with an increase of the σ factor for Ni contributors only. As already observed for the dried materials, the error bar on Si contributors is quite important. This decrease of the apparent number of Ni and Si and the increase of the corresponding σ are well accounted for by the decomposition of the supported phyllosilicate phase. Thus IR results[35] show that after vacuum treatment at 700 °C, the structural hydroxyl groups of silica-supported phyllosilicates of talc and/or serpentine structure are destroyed, giving rise to Ni^{2+} ions better dispersed on the support. The Ni−Ni distances and Ni−Si are modified in comparison to the ones found for the dried materials. The value for the Ni−Ni distance is close to that obtained from X-ray diffraction for NiO (2.96 Å),[36] although the characteristic peaks of Ni oxide, in particular in the 4−5.5 Å, are not observed.

(b) INi(en)-700. The EXAFS signal for this sample (Figures 5A and 6A) compares to those observed for activated DPU and ENi(NH$_3$) samples, indicating that N and C atoms of ethanediamine are removed under the activating treatment and replaced by oxygen atoms of the support. The Fourier transform (Figures 5B and 6B) shows a two-peak oxygen first shell and a peak at around 2.7 Å indicating that, in contrast to INi(en)-80, Ni and Si ions are now present in the coordination sphere of Ni. The amplitude of the latter peak is markedly stronger than that observed for DPU and ENi(NH$_3$) samples.

The apparent number of Ni neighbors is shown to be rather close to that observed for ENi(NH$_3$)-700 while the apparent number of Si is larger (Table 2). The increase of amplitude of the signal in comparison to that of DPU and ENi(NH)$_3$ is due to the net decrease of the σ factor for Ni contributors. This phase appears less disordered than for the other materials (Figure 5A). In contrast, although the presence of Si contributors was necessary to get a correct fit, their contribution is affected by an important disorder (10^2 σ$_{Si}$ = 12.5) (Table 2).

As observed for DPU and ENi(NH$_3$), the Ni−Ni distance is close to that found for NiO. However, for this compound, the existence of small size NiO particles may be accounted for by the presence of small contributions around 3.8, 4.5, and 5.3 Å corresponding to the ones observed for NiO (note that the distances indicated here are qualitative as multiple scattering may occur in this range).

It must be emphasized that for these last three compounds the Ni−Ni signal is kept. Therefore, the Ni^{2+} ions in these compounds cannot be considered as well dispersed.

(c) ENi(en)-700. The EXAFS spectrum of ENi(en)-700 displays a highly disordered structure (Figures 5A and 6A) and

(34) Swink, N. L.; Atoji, M. *Acta Crystallogr.* **1960**, *13*, 639−643.

(35) Kermarec, M. Unpublished results.
(36) Wyckoff, R. W. G. *Crystal Structures*; Wiley & Sons: New York, 1965; Vol. 1, pp 85−92.
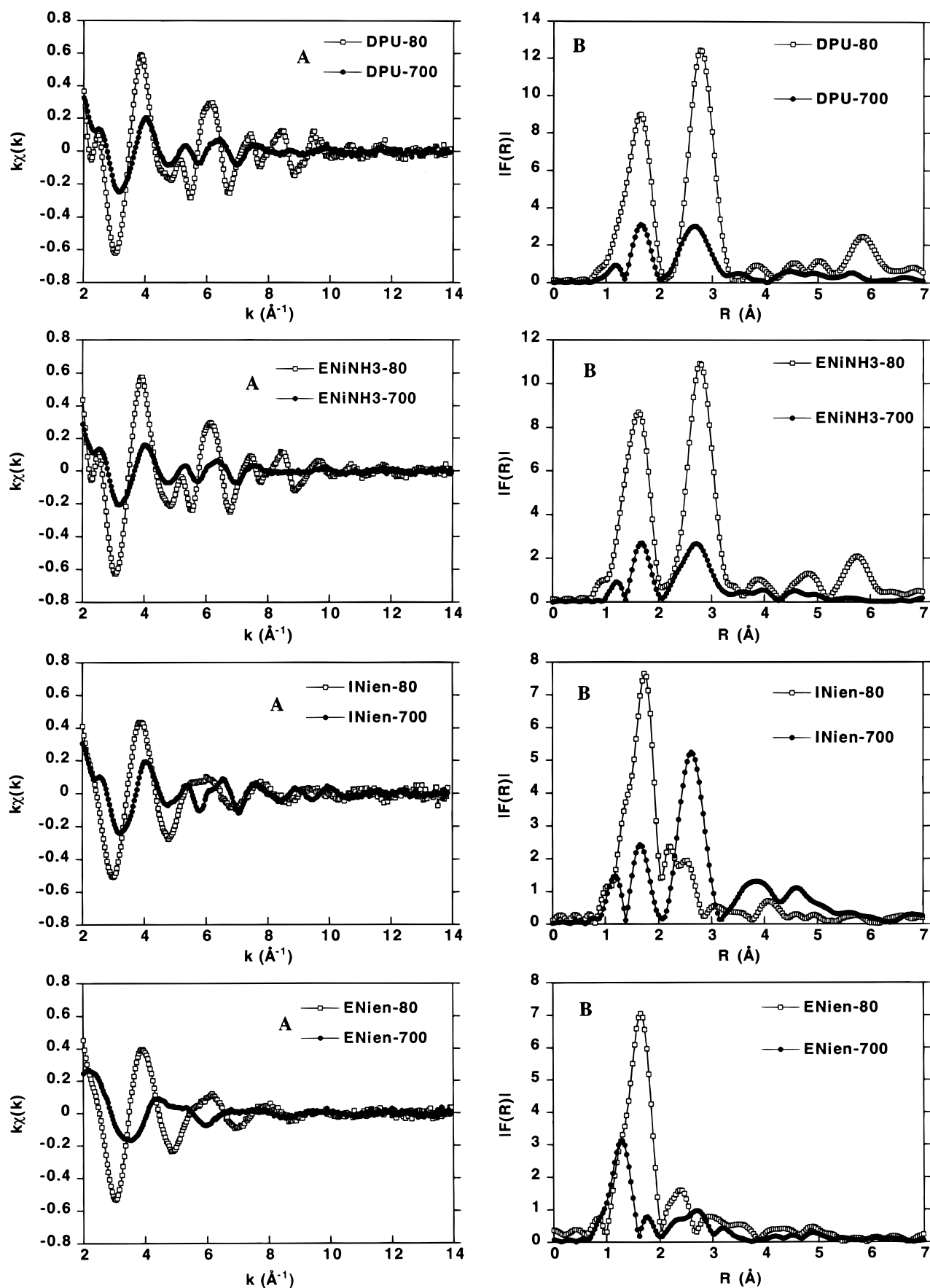
Figure 5. Comparison of the EXAFS signals (A) and Fourier transforms (B) of the dried (80 °C) and vacuum activated (700 °C) samples.

is strongly modified as compared with that of ENi(en)-80. The Fourier transform (Figures 5B and 6B) shows a two-peak

oxygen signal with inverse intensities in comparison with the other pretreated samples, together with a small structure around
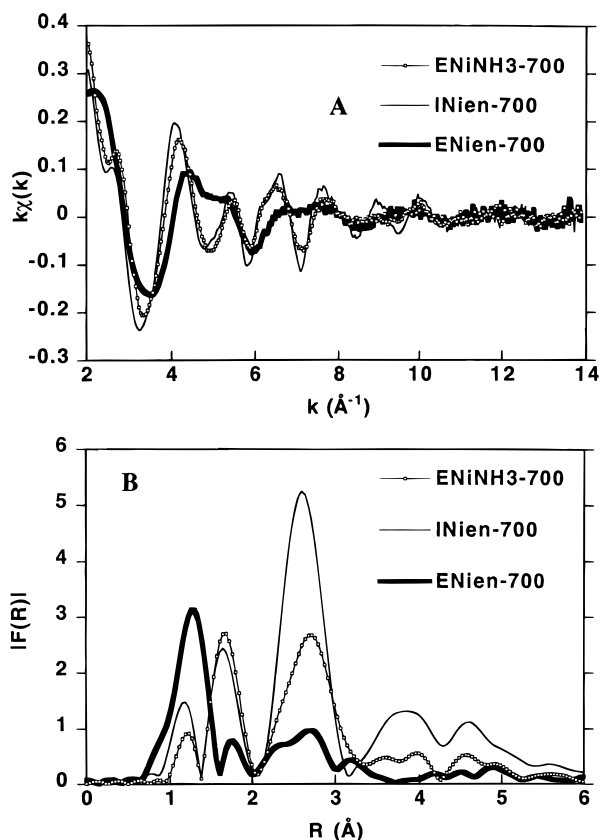
Figure 6. EXAFS signals (A) and Fourier transforms (B) of samples after a vacuum activating pretreatment at 700 °C.

Figure 7. Filtered second shell of ENi(en)-700: Ni contributors (A) and Si contributors (B).

2.7 Å. As for INi-700, the activating pretreatment at 700 °C has removed the N and C ligands which are replaced by oxygen atoms of the support. One can observe a weak peak of oxygen atoms around 1.9 Å and a major peak around 1.2 Å corresponding to $O_{(2)}$ atoms at a shorter distance. The values found for the apparent number of $O_{(1)}$ and $O_{(2)}$ are to be taken in consideration together with the corresponding σ values and their error bars (Table 2). The higher values found for σ_{O1} (0.08 (0.1)) against σ_{O2} (0.05 (0.03)) show that the signal corresponding to the short Ni$-O_2$ distance is predominant.

Considering now the very weak intensity of the second peak around 2.7 Å, the reliability of its fit appears highly questionable. However, we have tried to model this filtered second shell with FEFF parameters as either Ni or Si contributors (Figure 7, parts A and B, respectively).

Although similar values are found for the ρ^* agreement factors (Table 2), one can observe that the amplitude of the Si signal is significantly more adapted to fit the experimental signal. The quantitative results obtained when a Ni shell is modeled are obviously irrelevant: the abnormally high value found for σNi (0.18) indicates that the Ni signal would be very weak. This analysis indicates that Si rather than Ni contributors are present. Thus, the absence of Ni second neighbors sets ENi-(en)-700 apart in the series and selects it as *the compound with the best dispersion. The Ni^{2+} ions of ENi(en)-700 may be considered as isolated.*

(B) Edge Analysis. The analysis of the structures in the near-edge part of the absorption spectrum can provide information on the symmetry and the oxidation state of the Ni ions in the model compound and silica-supported materials. The spectra exhibit two regions: the preedge peak corresponding to transitions of 1s photoelectron to bound empty levels involving metallic orbitals[37,38] with partly 3d character and the main edge
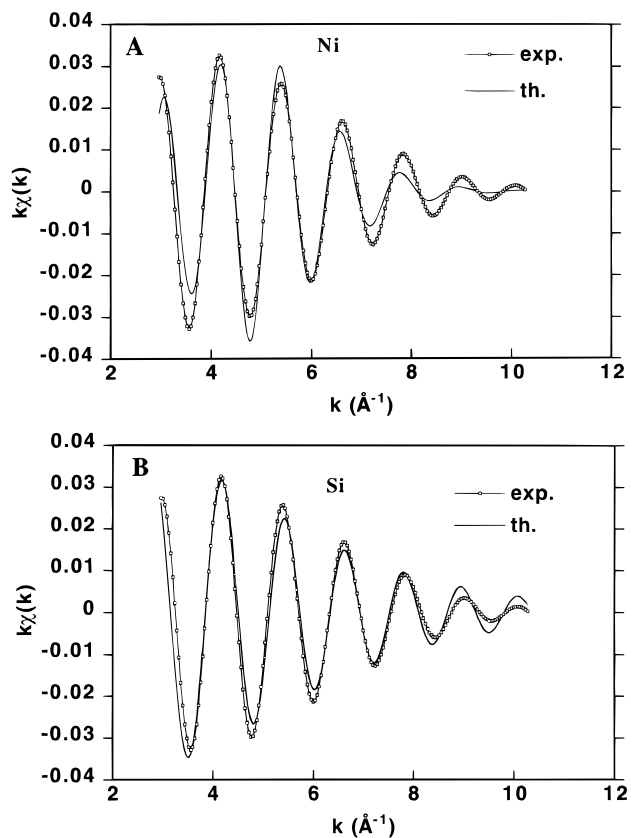
peak corresponding to transitions 1s → p symmetry levels hereafter referred to as 1s → 4p. The intensity for the preedge peak is related to the symmetry, the intensity being smaller for octahedral than for tetrahedral symmetry of the Ni environment. Figure 8 shows the edge spectra for dried and activated ENi-(NH$_3$) (Figure 8A) and ENi(en) samples (Figure 8B). We do not present here the edge spectrum for DPU and INi as they are quasi-identical to that of ENi(NH$_3$).

The edge (XANES) spectrum observed for ENi(NH$_3$)-80 is very similar to that found for Ta-25 (not shown here). The slight feature in the rising edge, before the main edge peak, could be related to a distortion of the octahedral coordination. In natural crystalline phyllosilicates where the distortion is greater, a net shoulder is observed.[32] The activation treatment at 700 °C strongly decreases the intensity of the main edge peak and that of the first EXAFS oscillation. In addition, this oscillation is shifted to higher energies. The intensity of the preedge peak is also increased.

All these features are consistent with the following interpretation: the nickel coordination sphere is moving from a quasioctahedral NiO$_6$ surrounding with long Ni$-O$ distances ($d \approx 2.05$ Å) (*dried samples*), to a much less symmetrical and less coordinated nickel environment with long and shorter Ni$-O$ distances ($d \approx 2.05$ and 1.75 Å) (*activated samples*). We can now discuss the features described above:

(a) The shift to higher energies of the first EXAFS oscillation is due to the shortening of Ni$-O$ distances and the decrease of its intensity is related to the decrease of the number of neighbors.

(b) The decrease of the height of the main edge peak is due to (i) the lowering of the initial O_h symmetry (the final symmetry

(37) Bianconi, A. *X-ray Absorption*; Koningsberger, D. C., Prins, R., Eds.; J. Wiley and Sons: New York, 1988; pp 573−662.

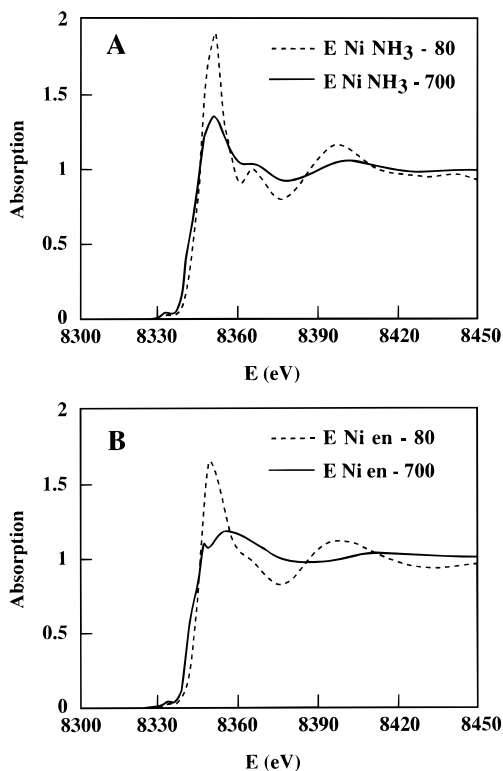(38) Cartier, C.; Verdaguer, M. *J. Chim. Phys.* **1989**, *86*, 1607−1621

Figure 8. Comparison of the edge spectra of ENi(NH₃) (A) and ENi-(en) (B) before and after pretreatment at 700 °C.

C_{3v}, D_{3h}, or even C_s will be discussed in the subsequent section) and the corresponding splitting in energy of the p levels; (ii) the stronger mixing of the metal p orbitals with the ligands containing orbitals since the ligands are at shorter distances; and (iii) some sharing of the p metallic orbitals between the two molecular orbital levels involving the 3d and the 4p metallic orbitals. This last point is confirmed by the increase in intensity of the preedge peak (due to 4p mixing). Such observations (decrease of the intensity of the main edge peak and of the first EXAFS oscillation, shift of this EXAFS oscillation toward higher energies, and increase of the intensity of the preedge peak) are common when moving from octahedral to tetrahedral complexes.[39]

However, for samples giving rise to phyllosilicate-like structures, it may be pointed out that the general shape of the edge spectra remains similar for the dried and activated samples and that the energy of the main edge peak remains practically unchanged. This strongly suggests that a large part of the nickel ions remains in octahedral symmetry.

In contrast to samples giving rise to phyllosilicate-like structures, ENi(en) is strongly modified after the activation treatment (Figure 8B). The XANES spectrum of ENi(en)-80 shows the classical white band characteristic of an octahedral symmetry, while that of ENi(en)-700 does not resemble that found for Ni^{2+} ions in a 6-fold site. It exhibits a marked peak at 8347.2 eV and a flatter main edge peak with a much lower intensity than that observed for the other activated samples. As for the other compounds, an increase of the intensity of the preedge peak is also observed. The shift of the first EXAFS oscillation toward higher energies is even more visible for this sample, and accounts for the shorter Ni−O$_{(2)}$ distance (Table 2).

To summarize, these observations agree with a decrease of the average coordination number (lowering of the initial O_h

symmetry) together with a distribution of the Ni−O distances. For ENi(NH₃)-700, DPU-700, and INi-700 samples, the major part of Ni^{2+} ions remains in octahedral symmetry, while for ENi(en)-700, the different shape found for the main edge curve suggests that the majority of Ni^{2+} ions with O$_{(2)}$ atoms at short distance are in a lower symmetry.

Discussion

In the preceding section, we have shown that the activation treatment leads to a lowering of the Ni coordination number and of the symmetry of the Ni site, with a distribution of two Ni−O distances for all samples. We have now to interpret the short Ni−O$_{(2)}$ and long Ni−O$_{(1)}$ distances and to determine the structure of the Ni site grafted on the silica support. The estimation of the average coordination number from EXAFS has been shown to be poor, owing to the inaccuracy on the number of oxygen atoms in the same shell at different distances. To solve these problems, experiments in DRS spectroscopy have been performed on the activated samples on one hand, and the structure of the Ni site grafted on the support has been modeled by using ab initio calculations based on the Density Functional Theory (DFT) on the other hand.

Interpretation of the Short Ni−O$_{(2)}$ Distance. Shorter metal−oxygen distances may be related either to an increase of the oxidation state, i.e., to the presence of Ni^{3+} ions, or to a decrease of the Ni coordination number. The presence of Ni^{3+} ions has already been assumed for other Ni-containing systems studied by EXAFS.[40−42] In those systems involving TiO₂ support, the presence of Ni^{3+} ions is chemically favored. Thus, this latter support gives rise to O$_2^{2-}$ species[43] permitting the stabilization of Ni^{3+}−O$_2^{2-}$ complexes. Silica is not known to stabilize the higher oxidation degrees for nickel. Indeed, the oxidation of Ni^{2+} ions into Ni^{3+} ions in the course of a vacuum activating treatment at 700 °C is highly questionable. Other arguments rule out the existence of Ni^{3+} ions. Thus, the position of the preedge peak is not compatible with the presence of a quantitative amount of Ni^{3+} ions as this peak is shown to be slightly shifted toward lower energies (−0.4 eV) instead of being shifted toward higher energies. Manceau and Calas[32] reported on for LaNiO₃ an upward shift of the preedge peak by 2 eV as compared with that observed for Ni^{2+}-containing phyllosilicates. In addition, it is well-known that isolated Ni^{3+} ions, which have a larger UV extinction coefficient than that of Ni^{2+} ions, give rise to intense d−d bands in the 320−305 and 415−460 nm range.[44,45] Thus very intense UV−visible bands in this range should be found for the ENi(en)-700 sample and this was not observed.

The second hypothesis to explain the existence of shorter distances is the decrease of the coordination number, due to a weaker steric hindrance. In ionic materials, with Ni in 4-fold coordination, the Ni−O distance is about 1.95 Å. Distances in the 1.8−1.85 Å are even found for Ni complexes with square-planar coordination.[46−48] In our materials, the Ni−O₂ distance

(39) Briois, V.; Lequan, R. M.; Lequan, M.; Cartier, C.; Van Der Laan, G.; Michalowicz, A.; Verdaguer, M. *Chem. Mater.* **1992**, *4*, 484−493.

(40) McBreen, J.; O'Grady, W. E.; Pandya, K. I.; Hoffman, R. W.; Sayers, D. E. *Langmuir* **1987**, *3*, 428−433.
(41) Espinose, J. P.; Gonzalez-Elipe, A. R.; Caballero, A.; Garcia, J.; Munuera, G. *J. Catal.* **1992**, *136*, 423−431.
(42) Pickering, I. J.; George, G. N.; Levandowski, J. T.; Jacobson, A. J. *J. Am. Chem. Soc.* **1993**, *115*, 4137−4144.
(43) Che, M.; Tench, A. J. *Adv. Catal.* **1983**, *32*, 1−148.
(44) McClure, D. S. *J. Chem. Phys.* **1962**, *36*, 2757−2779.
(45) Lo Jacono, M.; Sgamellotti, A.; Cimino, A. *Z. Phys. Chem. Neue Folge* **1970**, *70*, 179−194.
(46) Shibata, S.; Kishita, M.; Kubo, M. *Nature* **1957**, *179*, 320−321.
(47) Stewart, J. M.; Lingafelter, E. C. *Acta Crystallogr.* **1959**, *12*, 842−845.

($d \approx 1.75$ Å) is significantly shorter showing that this symmetry is not suitable. Moreover a D_{4h} symmetry for the surface Ni complex should probably give rise to smaller preedge peaks.

A previous work using diffuse reflectance spectroscopy (DRS) indicated a distorted tetrahedral symmetry for a ENi(NH$_3$) sample activated in flowing oxygen treatment at 500 °C while an activation under vacuum at 700 °C led to Ni^{2+} ions assumed to be 3-coordinated (Ni$^{2+}_{3c}$ ions) in D_{3h} or C_{3v} symmetries.[12] Recent DRS results on our samples pretreated in flowing oxygen at 500 °C were interpreted by the presence of a majority of 4-coordinated Ni^{2+} ions (Ni$^{2+}_{4c}$ ions). After activation in a vacuum at 700 °C, new d−d transitions corresponding to a lower symmetry were observed.[23] Calculations of the transitions were performed for a Ni^{2+} ion in a dehydrated A-zeolite assuming a D_{3h} geometry.[49−50] Although the best fit between our experimental transitions and theoretical calculations for a Ni^{2+} ion in a D_{3h} symmetry was obtained from Polak and Cerny's data,[50] some discrepancies remain. In the absence of theoretical calculations based on other symmetries (C_{3v} or C_s), the structure of the Ni site cannot be deduced from DRS data. Hence, it may only be inferred that an activating vacuum treatment at 700 °C lowers the coordination and the symmetry in comparison with the activating treatment at 500 °C, giving rise to Ni$^{2+}_{3c}$ ions.

Table 3. Fitted $d_{Ni−O}$ Distances Calculated in DFT* for Ni$^{2+}_{3c}$ Ions Grafted on Modeled Si$_2$O$_3$H$_4$ and Si$_5$O$_8$H$_8$ Sites[a]

modeled site of silica	$d_{Ni−O1}$ (Å)	$d_{Ni−O2}$ (Å)	$d_{Ni−O2}$ (Å)
Si$_2$O$_3$H$_4$	3.21	1.79	1.80
Si$_5$O$_8$H$_8$	2.01	1.82	1.83

[a] The calculations are performed with use of the LDA (Local Density Approximation) and the B88 (corresponding to the Becke exchange correction) corrections.[51]

Structure of the Ni Sites. The existence of two different distances may be interpreted according to the following hypotheses. (i) Ni^{2+} ions may be located in different types of sites, one corresponding to large Ni−O$_{(1)}$ distances ($d_{Ni−O} \approx 2$ Å), the other one to short Ni−O$_{(2)}$ distances ($d_{Ni−O} = 1.74−1.76$ Å). The first category may correspond to hexacoordinated Ni^{2+} ions since the Ni−O distance is close enough to that encountered for bulk NiO ($d = 2.09$ Å). The second one could be assigned to isolated Ni$^{2+}_{3c}$ ions as shown for ENi(en)-700. (ii) a variant of hypothesis (i) infers that the site corresponding to Ni$^{2+}_{3c}$ ions may be distorted, with a distribution of short and long Ni−O distances. (iii) All Ni^{2+} ions are 3-coordinated in a distorted site with different Ni−O distances.

This last hypothesis has to be discarded as the edge data of activated ENi(NH$_3$), DPU, and INi(en) samples show that some Ni^{2+} ions remain in octahedral symmetry. In our laboratory, recent ab initio calculations with DFT theory have been carried out to model the sites which can accommodate Ni$^{2+}_{3c}$ ions on amorphous silica.[51] There exist a large variety of sites (SiO)$_n$ at the surface of an amorphous silica. The simplest site permitting the grafting of Ni on the surface of silica, labeled Si$_2$O$_3$H$_4$, may be represented by 2SiO$_4$ tetrahedra sharing a bridged oxygen atom (Figure 9a). This scheme with 3 oxygen atoms was already assumed by Bonneviot and co-workers to be the coordination site for the Ni^{2+} metallic center.[12] The results of modeling show that the Ni^{2+} ion interacts only with
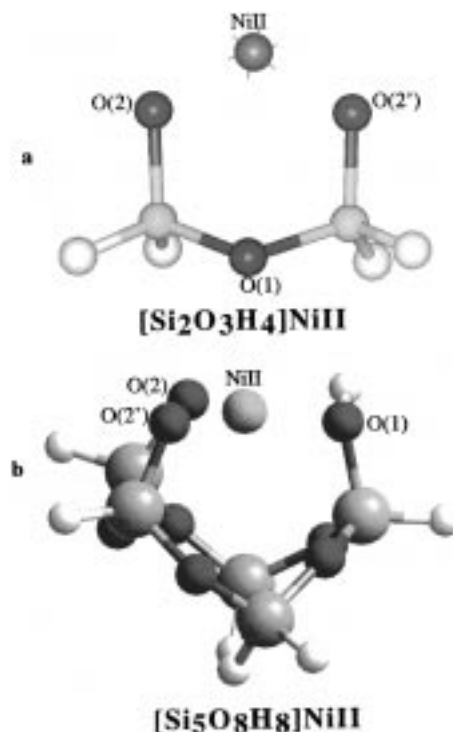
(48) Frasson, E.; Panattoni, C.; Sacconi, L. *J. Phys. Chem.* **1959**, *63*, 1908−1911.
(49) Klier, K.; Ralek, M. *J. Phys. Chem. Solids* **1968**, *29*, 951−957.
(50) Polak, R.; Cerny, V. *J. Phys. Chem. Solids* **1968**, *29*, 945−950.
(51) Garrot, J. M. Thesis, 1996, Université P. et M. Curie.

Figure 9. Scheme of Ni^{2+} ion grafted onto modeled Si$_2$O$_3$H$_4$ (a) and Si$_5$O$_8$H$_8$ (b) sites of an amorphous silica.

the two terminal oxygen atoms located at 1.8 Å, while the bridged oxygen is at 3.21 Å from the Ni^{2+} ion (Table 3). In contrast, the tricoordinated structure for the Ni^{2+} ion is well accommodated by the Si$_5$O$_8$H$_8$ site (Figure 9b). This latter site is flexible enough to allow the relaxation of Ni^{2+} ions in the plane of the 3 oxygen atoms. The calculated distances (Table 3) in agreement with the experimental EXAFS distances correspond to a Ni$^{2+}_{3c}$ site in a trigonal distorted symmetry, with two short Ni−O$_{(2)}$ distances ($d_{NiO} = 1.82−1.83$ Å) and a larger one Ni−O$_{(1)}$ ($d_{NiO} = 2.01$ Å).

Thus, the existence of two Ni−O distances is well accounted for by hypothesis (ii) with two sites corresponding to Ni$^{2+}_{6c}$ ions ($d_{Ni−O} = 2−2.04$ Å) and to Ni$^{2+}_{3c}$ ions in a highly distorted site ($d_{Ni−O(1)} = 1.99−2.04$ Å and $d_{Ni−O(2)} = 1.74−1.76$ Å).

Dispersion of the Supported Ni Phase. The dispersion of these activated supported materials is related to the amount of Ni second neighbors, the lower the number of Ni backscatterers the higher the dispersion. If no Ni backscatterers are detected at a distance lower than 4 Å, the Ni^{2+} ions can be considered as isolated. Owing to the disordered structures produced by the activating treatment, the difficulty to estimate reliable values for the apparent number of atoms located within a shell comprising more than one category of backscatterers has already been underlined. This is the case for the first (O$_{(1)}$ and O$_{(2)}$) and second shells (Ni and Si) for the activated samples. For this reason, neither the number of O$_{(1)}$ and O$_{(2)}$ atoms nor the proportion of larger and shorter Ni−O distances for each compound can be precisely evaluated. EXAFS spectroscopy is not relevant to estimate with accuracy the proportion of the 6- and 3-coordinated Ni phases, particularly in highly disordered phases.

However, for DPU, ENi(NH$_3$), and INi(en) samples activated at 700 °C, we have shown that Ni backscatterers are present in a significant amount characteristic of an ill-dispersed phase. In contrast, ENi(en)-700, despite its highly disordered structure, has been shown to have Si rather than Ni second neighbors and appears therefore as the best dispersed material.

Table 4. Nature of the Phase or Ions Produced as a Function of the Mode of Deposition and the Activating Treatment

	samples	
	dried	activated
mode of deposition		
ENi(NH)₃	Ni^{2+}_{6c} (supported phyllosilicate)	Ni^{2+}_{6c} small NiO particles (predominant phase) Ni^{2+}_{3c}
DPU	Ni^{2+}_{6c} (supported phyllosilicate)	Ni^{2+}_{6c} small NiO particles (predominant phase) Ni^{2+}_{3c}
ENi(en)	$[Ni(en)_3]^{2+}$ electrostatically adsorbed	Ni^{2+}_{3c} isolated ions only
INi(en)	$[Ni(en)_3]^{2+}$ electrostatically adsorbed	Ni^{2+}_{6c} small NiO particles (predominant phase) Ni^{2+}_{3c}

Nature of the Hexacoordinated Ni Phase. (a) DPU and ENi(NH₃). Supported Ni phyllosilicates (DPU-80 and ENi-(NH₃)-80 samples) have a brucitic Ni hexacoordinated phase. To understand the decomposition of supported Ni phyllosilicates, it is first necessary to know the phases resulting from the decomposition of bulk Ni phyllosilicates.

It is known that the decomposition of synthetic phyllosilicates, which occurs by dehydroxylation of the structural OH groups, depends on the crystallinity of the material.[28,52] The decomposition of nepouite occurs at lower temperatures than those observed for talc[53,54] owing to the better accessibility of structural OH groups. For a crystalline nepouite, DRX patterns identify after thermal treatment in air at 1050 °C an amorphous silica phase and NiO. For talc decomposed at 1100 °C, an amorphous silicate is observed but not identified, some diffraction lines corresponding to NiO.[53] At higher temperatures, recrystallization of silica and of the amorphous silicate in cristobalite and olivine is observed.[54] The mechanism of dehydroxylation has been extensively studied on Mg talcs[55,56] only. At high temperature, enstatite and cristobalite are produced. During dehydroxylation, the loss of protons in some regions of talc is compensated by the migration of cations,[57] yielding the new silicate phase. The initial layer silicate is supposed to transform in a double and single chain silicate of amphibole and pyroxene-types.[58] However, no dispersed Ni²⁺ ions are generated.

Assuming the same type mechanism of dehydroxylation for silica-supported Ni phyllosilicates, the formation of a chain silicate involves a decrease of the dimensionality of the supported silicate, which is compatible with the decrease of the number of Ni and Si observed after the activation pretreatment. During the decomposition of the supported silicate, some Ni²⁺ ions could migrate toward the support giving rise to dispersed Ni^{2+}_{3c} ions grafted on silica. *Thus, the support helps for the fixation of dispersed Ni²⁺ ions, in contrast to the behavior of bulk phyllosilicates which do not generate isolated ions after decomposition.*

Turning now to the 6-coordinated phase, the presence of an amorphous silicate and/or a NiO phase supported on silica may be considered on the basis of Ni−Si and Ni−Ni distances. The activation pretreatment strongly decreases the number of Ni and Si neighbors and shortens the Ni−Ni and Ni−Si distances (2.97 and 3.12−3.18 Å, respectively). The Ni−Si distance does not correspond to the average distance in silicates of known structure such as olivine or pyroxene-type silicates ($d_{Ni-Si} = 3.24$ Å), which rules out the existence of a well-characterized silicate

phase. The Ni−Ni distance corresponds to that of NiO, although the peaks at $R > 3.5$ Å characteristic of this phase are not observed. These features may be explained by the formation of very small NiO particles in a highly disordered system. The weak apparent number found for Si ($N_{Si} = 1.1-1.6$) suggests that Ni is probably grafted on the silica support.

(b) INi(en) and ENi(en). EXAFS analysis shows that in the dried samples, Ni²⁺ ions keep their (en) ligands and are not grafted onto the silica support. After an oxidizing step at 500 °C followed by vacuum pretreatment at 700 °C, the EXAFS spectra of these samples markedly differ. As mentioned in the preceding paragraphs, ENi(en)-700 gives rise to a preponderant phase constituted of isolated Ni^{2+}_{3c} while the impregnated sample leads to an ill-dispersed Ni phase with NiO particles of small size. The reasons for these different behaviors have to be investigated in the initial steps of the preparation. These preparation modes differ by the washing step which is performed for the exchange process only. For both materials, the (en) ligands are oxidized under flowing oxygen at 500 °C, allowing grafting of Ni²⁺ ions on Si−O−Si or Si(OH) groups. For INi-(en), the excess of adsorbed nitrate within the pores of silica is subsequently transformed into small NiO particles.

Table 4 reports on the nature of the supported phase as a function of the mode of Ni deposition and the activating treatment. It clearly appears that exchange with ethanediamine may be selected as the best route to generate isolated Ni^{2+}_{3c} ions.

Conclusion

EXAFS spectroscopy was employed to follow the coordination sphere of silica-supported Ni complexes from the initial step (dried samples) to the final material (activated samples). In this work, EXAFS was shown to be a suitable probe of the metal−support interactions in line with earlier data.[59] The chelating ethanediamine ligand was selected to protect the coordination sphere and avoid the secondary reactions leading to supported phyllosilicates observed when ammine ligands are used. A higher proportion of isolated Ni²⁺ ions was therefore expected. Four modes of deposition of nickel were compared, two leading to the formation of supported talc-like and serpentine-like silicates (ENi(NH₃) and DPU samples respectively) and the other two using the (en) ligand leading to Ni complexes in electrostatic interaction with the support (*dried materials*).

After vacuum treatment at 700 °C (*activated materials*), all samples yield various proportions of isolated Ni^{2+}_{3c} ions in a distorted site with a distribution of long ($d_{Ni-O(1)} = 1.95-2.04$ Å) and short ($d_{Ni-O(2)} = 1.74-1.76$ Å) distances, and Ni^{2+}_{6c} ions in octahedral symmetry. In contrast to previous results obtained on similar samples,[9,11,17,18] the fitted structural param-

(52) Carriat, J. Y.; Che, M.; Kermarec, M. *Catal. Lett.* **1994**, *25*, 127−140.

(53) Martin, G. A.; Renouprez, A.; Dalmai-Imelik, G.; Imelik, B. *J. Chim. Phys.* **1970**, *67*, 1149−1160.

(54) Wendt, G.; Siegel, H.; Schmitz, W. *Cryst. Res. Technol.* **1982**, *17*, 1434−1441.

(55) Weselowski, M. *Thermochim. Acta* **1984**, *78*, 395−421.

(56) Daw, J. D.; Nicholson, P. S.; Embury, J. D. *J. Am. Ceram. Soc.* **1972**, *55*, 149−151.

(57) Nakahira, M.; Kato, T. *Clays Clay Miner.* **1964**, *12*, 21−27

(58) Avgustinik, A. I.; Tandura, P. Z.; Sverchkova, L. I. *Zh. Prikl. Khim.* **1949**, *22*, 1150−1959.

(59) Tan, B.-J.; Klabunde, K. J.; Tanaka, T.; Kanai, H.; Yoshida, S. *J. Am. Chem. Soc.* **1988**, *110*, 5951−5958. Van Zon, F. B. M.; Maloney S. D.; Gates, B. C.; Koningsberger, D. C. *J. Am. Chem. Soc.* **1993**, *115*, 10317−10326. Tauster, S. J.; Fung, S. C.; Garten, R. L. *J. Am. Chem. Soc.* **1978**, *100*, 170−175. Horsley, J. A. *J. Am. Chem. Soc.* **1979**, *101*, 2870−2874.

eters are determined with the corresponding error bars. It is shown that EXAFS spectroscopy permits the detection of the presence of different categories of atoms in the first (oxygen backscatterers) and second (Ni and Si backscatterers) shells but fails to determine with accuracy the proportions of these various contributors and of the 3- and 6-coordinated Ni phases.

For DPU and ENi(NH$_3$) samples, these phases originate through the decomposition of the initial supported phyllosilicates. The hexacoordinated phase characterized by Ni−O(1) distances around 2−2.04 Å is predominant and has been attributed to very small particles of NiO on the silica surface.

When the (en) chelating ligand is used, both impregnation and exchange methods lead after pretreatment at 700 °C to isolated Ni$^{2+}_{3c}$ ions grafted onto the support. However, the impregnation method generates a majority of small NiO particles through the decomposition of Ni (en) nitrate. Depending on the use of the reduced final catalyst, the (en) ligand proves its supremacy in the exchange method, which produces isolated Ni$^{2+}_{3c}$ ions only. These ions may be photoreduced into Ni$^+$ ions with the highest reduction degree ever found (40%).[60] The interest of the impregnation method with Ni (en) nitrate is to generate much smaller NiO particles and correlatively, after reduction, Ni particles (20 Å) smaller than those observed in the case of impregnation with Ni nitrate (60 Å).[4,61]

(60) Carriat, J. C.; Lepetit, C.; Kermarec, M.; Che, M. *J. Phys. Chem.* Accepted for publication.

(61) Cheng, Z. X.; Louis, C.; Che, M. *Preparation of Catalysts VI*; Poncelet, G., Martens, J., Delmon, B., Jacobs, P. A., Grange, P., Eds.; Elsevier: Amsterdam, 1995; pp 1027−1036.